Polym. Bull. (2012) 68:1663–1675
DOI 10.1007/s00289-011-0665-y

ORIGINAL PAPER

Preparation and characterization of exfoliated poly(vinyl acetate-co-methyl methacrylate)/Cloisite 30B nanocomposite

M. Mohsen-Nia · F. S. Mohammad Doulabi

Received: 27 April 2011 / Revised: 15 October 2011 / Accepted: 1 November 2011 /
Published online: 9 November 2011
© Springer-Verlag 2011

Abstract Poly(vinyl acetate-co-methyl methacrylate)/Cloisite 30B, P(VAc-co-MMA)/C30B nanocomposite have been prepared via emulsion polymerization method. In the nanocomposite latex preparation sodium lauryl sulfate, ammonium persulfate, and poly(vinyl alcohol) were as anionic emulsifier, conventional anionic initiator, and stabilizer, respectively. The resulting P(VAc-co-MMA)/C30B nanocomposites with various filler contents were characterized using elemental analysis, Fourier transform infrared spectroscopy, X-ray diffraction (XRD), scanning electron microscopy, transmission electron microscopy (TEM), and atomic force microscopy. The effects of various C30B contents on the polymerization rate and monomer conversion of P(VAc-co-MMA)/C30B were studied. Thermal properties of the nanocomposite were studied by dynamic mechanical thermal analysis. The XRD and TEM results demonstrated that the synthesized polymer chains were aggregated into the C30B interlayer regions and consequently complete exfoliation was produced.

Keywords Nanocomposite · Emulsion polymerization · P(VAc-co-MMA)/C30B · Exfoliation · Dynamic mechanical thermal analysis

M. Mohsen-Nia (✉)
Department of Chemical Engineering, University of Kashan, Kashan, Iran
e-mail: moh.moh@cheme.caltech.edu

M. Mohsen-Nia
Division of Chemistry and Chemical Engineering, Caltech, Pasadena, CA, USA

F. S. Mohammad Doulabi
Department of Chemistry, University of Kashan, Kashan, Iran

Introduction

During the past decade, there have been significant works directed toward the elaboration of nanocomposite materials by embedding inorganic particles in the polymer matrices [1–3]. The polymer microstructure has a strong influence on the bulk chemico-physical properties of the polymer. Polymers that contain only a single type of monomer are known as homopolymers, while polymers containing a mixture of monomer are known as copolymers [4]. The copolymerization of vinyl acetate and acrylic monomers (acrylic acid, methyl acrylate, butyl acrylate, and acrylamide) produces useful copolymer latexes having a wide range of applications [5].

In polymer–inorganic nanocomposites, the properties of inorganic particles in terms of mechanical strength, modulus, and thermal stability are combined with the process ability and flexibility of polymer matrices [6, 7]. Nano-sized fillers, e.g., nanometer-thin platelets, such as clays have high potential for use in polymer–inorganic nanocomposites in which enhanced thermal and mechanical properties are required. The properties of polymer–inorganic nanocomposites can be affected by the polymers and nano-sized fillers microstructure as well as the dispersion feature of the nano-sized fillers in the polymer matrices [8].

Clays find wide range of applications in various areas of science. The clay that is most generally used is montmorillonite (MMT), which belongs to the 2:1 layered silicate. Its crystal lattice consists of two silica tetrahedral sheets fusing into an octahedral sheet. Isomorphic substitution within the layers (e.g., Al^{3+} replaced by Mg^{2+}) generates a negative charge that is counterbalanced by cations such as Ca^{2+} and Na^{+}. Therefore, MMT is only miscible with hydrophilic polymers, such as poly(vinyl alcohol) (PVA). To render MMT miscible with other polymers, many cationic-organic surfactants can be used to produce modified organoclays. C30B is a natural MMT modified with a quaternary ammonium salt. As the surface energy of the organoclay is much lower, many polymers and monomers can easily intercalate within the interlayer space [9]. Therefore, by using organoclays, different grades of polymer–inorganic nanocomposites with enhanced physicochemical properties can be prepared.

Depending on the structure of the clay dispersed in the polymer matrix, two different types of composites can be obtained. In the intercalated composites, polymer chains are inserted into the interlayer space of the stacking silicate platelets, but the silicate layers are still well ordered although the basal space is greatly expanded. In the exfoliated composites, the discrete clay layers are randomly dispersed in the continuous polymer matrices [10].

Poly(methyl methacrylate) (PMMA) is one of the most important acrylic polymers used widely because of its excellent clarity and good weathering behavior. It is hard, stiff, and brittle thermoplastic at room temperature. However, it has poor impact and solvent resistance, which restrict its applications [11].

The polymerization of vinyl acetate is particularly attractive for many industrial applications. Moreover, the copolymerization of vinyl acetate with other monomers such as methyl methacrylate produces useful latexes having a wide range of properties [4, 12]. Copolymers of vinyl acetate and acrylates in latex form are

excellent for interior and exterior paints and are superior to either homopolymer alone. Carboxylic acid monomers such as acrylic acid and methacrylic acid copolymerize with vinyl acetate in an enormous range of accessible copolymer compositions for modifying the final properties of the prepared latex films [13].

In this study, P(VAc-co-MMA)/C30B nanocomposites containing different filler loadings were prepared. The morphology of the prepared P(VAc-co-MMA)/C30B nanocomposite latex was investigated by Fourier transform infrared (FT-IR) spectroscopy, X-ray diffraction (XRD), scanning electron microscopy (SEM), transmission electron microscopy (TEM), and atomic force microscopy (AFM). The obtained results indicated that the polymerizing chains were aggregated into the C30B interlayer regions and consequently the exfoliation of C30B was completed. Thermal properties of the prepared nanocomposites were studied by dynamic mechanical thermal analysis (DMTA).

Experimental

Materials

Commercial grade of VAc, MMA were supplied from Iranian petrochemical Co. and PVA (degree of hydrolysis 88% degrees of polymerization 580) was supplied from Kuraray Chemical Co., Japan. The C30B was obtained from Southern Clay Products, USA. The C30B is a kind of MMT, modified with methyl tallow bis-2-hydroxyethyl quaternary ammonium chloride (MT_2EtOH), the cation exchange capacity (CEC) of C30B is 90.0 mequiv/100 g. Sodium lauryl sulfate (SLS 99%) was supplied by Fluka. Ammonium persulfate (APS) and sodium bicarbonate ($NaHCO_3$) were supplied by Merck Co. Inc., Germany. All chemicals were used without further purification. Water was distilled after being ion-exchanged.

Preparation of P(VAc-co-MMA)/C30B nanocomposites

P(VAc-co-MMA)/C30B nanocomposite with low C30B loading (1, 3, and 5 wt%) have been prepared via in situ emulsion polymerization. C30B was dispersed in 50 mL deionized water, and the dispersion was stirred vigorously overnight and then was dispersed by ultrasonication to prevent aggregation of nanoparticles. Then this solution was added to a glass three-neck reactor with a water jacket to maintain a constant temperature ±0.1 °C. The glass reactor was fitted with a reflux condenser, funnel, and mechanical stirrer. The speed of agitation with stirring was stable at 200–300 rpm. 47 g monomer containing vinyl acetate and methyl methacrylate poured into the dropping funnel, a quantity of distilled water was poured into the glass reactors then 0.1 g APS and 0.1 g buffer solution of $NaHCO_3$ were added and maintained under the constant agitation. The aqueous emulsified solution containing 2 g PVA and 0.2 g SLS were added to the reaction system. The mixture was stirred at 300 rpm and heated up to 75 °C. Afterward, the monomer mixture was added in drop wise to the reactor. The time of feeding was almost 80 min and after addition of the monomers, the polymerization was carried out

under nitrogen condition for 4 h. Then, the system was cooled to room temperature and the final latex was obtained without any post preparative treatments.

Characterization

The synthesized P(VAc-co-MMA)/C30B nanocomposites were studied by FT-IR spectroscopy and XRD. FT-IR were recorded by (magna 550; Nicolet) in the range of 4,000–400 cm^{-1} using KBr pellets. XRD patterns of the samples were collected on a Philips X'Pert MPD X-ray diffractometer with Cu-Kα radiation $\lambda = 1.54$ Å at a generator voltage of 40 kV and a generator current of 40 mA. All experiments were carried out in the reflection mode at ambient temperature with 2θ varying between 1 and 10°. The scanning speed was 1 min^{-1} and the step size was 0.01°.

Morphology observations

The surface morphology and particle diameters of the synthesized P(VAc-co-MMA)/C30B nanocomposite specimens were investigated using a scanning electron microscope (SEM, Philips). Before SEM examination, the samples were dried at room temperature and coated with a thin layer of gold, using a JEOL ion-sputter JFC-1100 coating machine. The morphology and C30B distribution nanocomposite were studied using TEM (Phillips CM-120 TEM) operating at an accelerating voltage of 120 kV. The shape and the morphological feature of the synthesized P(VAc-co-MMA)/C30B nanocomposite was studied using AFM (TS-150, Russia). In the AFM analysis, sample preparation is quite simple and does not require a conductive coating as for SEM [6].

Conversion

The conversion of the synthesized P(VAc-co-MMA)/C30B nanocomposite was determined by a gravimetric method. After monomer injection, the latexes samples were taken from the glass laboratory reactor at different times. Then, aqueous solution of hydroquinone (0.2 g, 0.5 wt%) were added to the glass vials containing the sample latexes. The vials were immersed in an ice bath for 15 min and then were placed in a desiccator for 1 h until they reach room temperature. The weight of wet latexes withdrawn were determined by using Sartorius analytical balance (model A200S, accurate to 0.0001 g). The samples were dried in a vacuum oven until constant weight was reached. Finally, the value of the dry mass was used for the conversion calculation of the synthesized P(VAc-co-MMA)/C30B nanocomposite.

Dynamic mechanical thermal analysis

DMTA storage modulus (E') and tanδ were obtained by a Rheometric Scientific PL-DMTA MkII and the temperature range studied was from −50 to 150 °C with a heating rate of 3 °C/min at 1 Hz of frequency. Samples were molded in $10 \times 7.45 \times 2$ mm^3 size. Glass transition temperatures, T_g of the nanocomposites

and pure polymer were determined from the maximum values in the tanδ versus temperature.

Results and discussion

Figure 1 shows the FT-IR spectra of (a) C30B and (b) P(VAc-co-MMA)/C30B, respectively. As shown in Fig. 1a absorption bands at around 3,632 cm^{-1} corresponds to the hydroxyl stretching that is bonded to the aluminum in clay. The peak maximum at 1,045 cm^{-1} is attributed to the Si–O in plane stretching. The peak for Si–O and Al(Al)OH bending vibration are observed at 463 and 919 cm^{-1}, respectively. The P(VAc-co-MMA)/C30B shows its characteristic absorption at 2,952 and 1,736 cm^{-1}, corresponding to C–H and C=O groups, respectively. The peaks at 1,445 and 1,243 cm^{-1} come from the C–H bending and C–O–C symmetrical vibration, respectively. The comparison of (a) spectrum with (b) shows that absorption peaks for C30B appearing in P(VAc-co-MMA)/C30B spectra. This result indicates the existence of P(VAc-co-MMA) in the C30B interlayers.

XRD method was used to characterize the formation and structure of the polymer–clay nanocomposite by monitoring the position, shape, and intensity of the

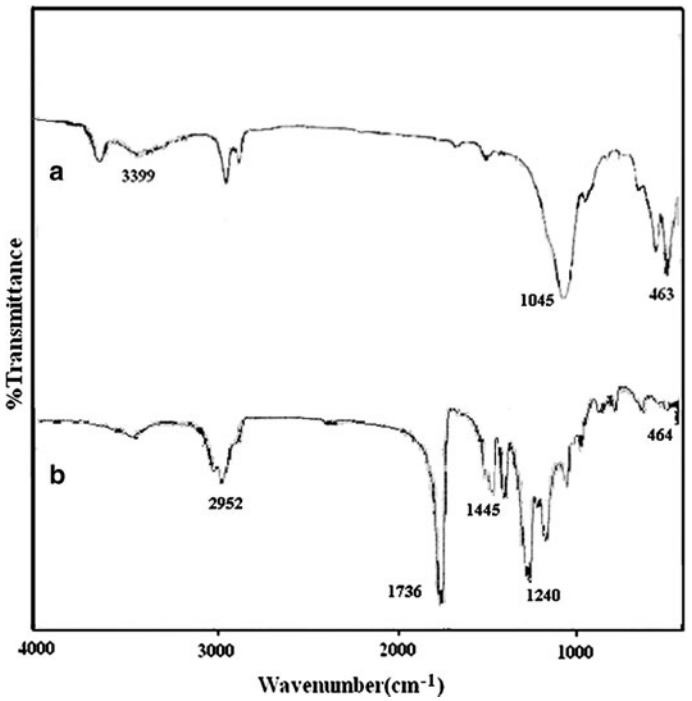

Fig. 1 FT-IR spectra of *a* C30B, *b* P(VAc-co-MMA)/C30B nanocomposite

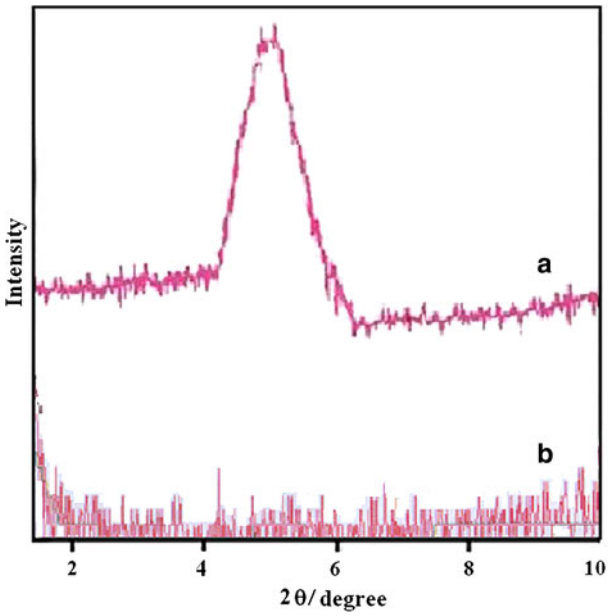

Fig. 2 XRD patterns of P(VAc-co-MMA)/C30B nanocomposite: *a* 1% C30B (non-exfoliated), *b* 3% C30B (exfoliated)

basal reflection from the silicate layers. In the polymer–clay nanocomposites, the polymer chains can be inserted between the silicate layers which increase the silicate interlayer volume and corresponding layer spacing. This increased layer spacing gives rise to the shifting of diffraction peaks to lower angles. So, diffraction peaks cannot be seen in the case of exfoliated structures where silicate layers are completely and uniformly dispersed in a continuous polymer matrix. Figure 2 compares the XRD patterns of the exfoliated and non-exfoliated P(VAc-co-MMA)/C30B nanocomposite samples, in this figure the non-exfoliated sample exhibits a single peak at an angle (2θ) of 4.92°. The characteristic diffraction peak disappeared for samples of the P(VAc-co-MMA)/C30B nanocomposite. This indicates that C30B has been fully exfoliated in the samples. It is found that in all systems the interlayer spacing increases due to the intercalation of copolymer into the layers of nano-C30B. Enhanced interlayer distance indicates that the layered structure is retained.

Figure 3 shows the results of SEM analysis of the synthesized P(VAc-co-MMA)/C30B nanocomposite. The SEM image indicates that no aggregates are present in the nanocomposite, according to this figure, the spherical molecules homogeneously dispersed and distributed randomly in surface. The particle size distribution is presented in Fig. 4. The coefficient of variation (Cv) which is a measure of the broadness of the particle size distribution was calculated using the following equations by counting at least 100 individual particles from SEM microphotographs.

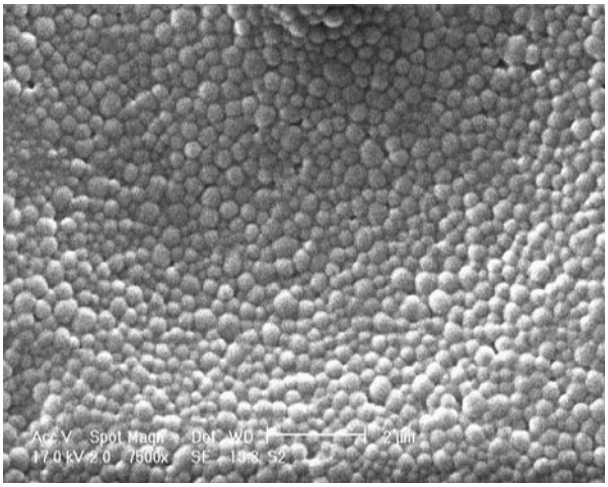

Fig. 3 SEM images of P(VAc-co-MMA)/C30B nanocomposite

$$\mathrm{Cv} = \frac{\left(\sum d_{\mathrm{i}} - \left(\sum n_{\mathrm{i}} d_{\mathrm{i}} / \sum n_{\mathrm{i}}\right)^2 \Big/ \sum n_{\mathrm{i}}\right)^{1/2}}{\left(\sum n_{\mathrm{i}} d_{\mathrm{i}} / \sum n_{\mathrm{i}}\right)} \times 100$$

where n_{i} is the number of particles with d_{i}.

The particle size of the synthesized P(VAc-co-MMA)/C30B nanocomposite is compared with that for the P(VAc)/C30B nanocomposite which is presented in the previous study [1].

According to Fig. 4, the size of particle was in the range of 100–400 nm and the average particle size is about 200 nm. The Cv was 16.40 by counting 150 particles

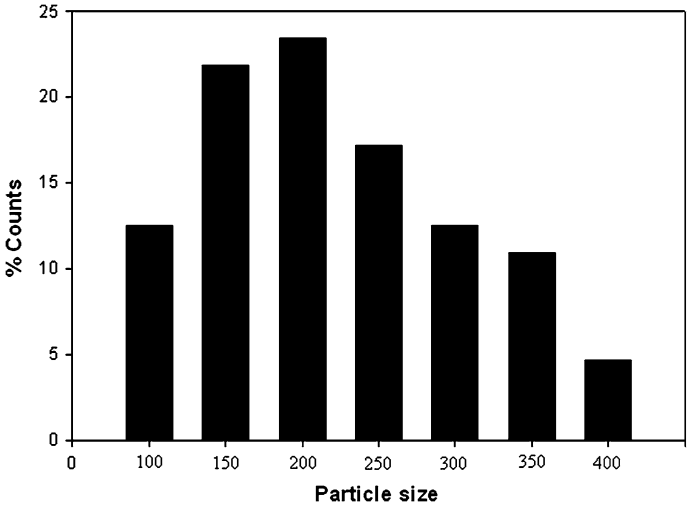

Fig. 4 Particle size distribution of P(VAc-co-MMA)/C30B nanocomposite

from the SEM micrographs. Figure 5 shows particle size distribution for the P(VAc)/C30B nanocomposite [1]. According to this figure, the size of particles was in the range of 100–400 nm and the average particle size is about 250 nm. The Cv was 14.10 by counting 150 particles from the SEM micrographs.

Figure 6 shows a TEM micrograph of P(VAc-co-MMA)/C30B nanocomposite having 3.0% wt of C30B, where the dark lines in the picture correspond to the C30B layers and P(VAc-co-MMA) copolymer appears as relatively gray/white domains.

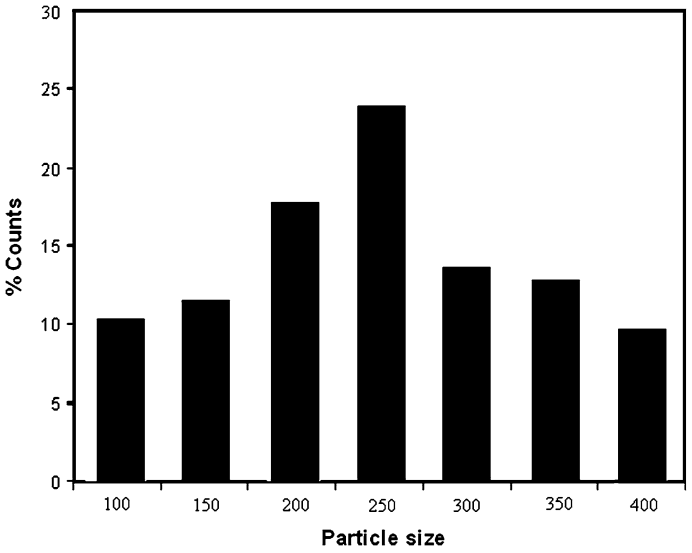

Fig. 5 Particle size distribution of P(VAc)/C30B nanocomposite

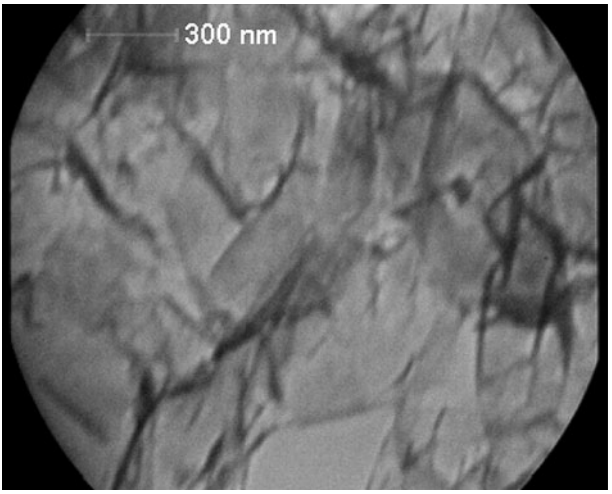

Fig. 6 Transmission electron microscopic (TEM) image of P(VAc-co-MMA)/C30B nanocomposite

It is clear that the C30B was well exfoliated, and the layers were dispersed in the polymer matrix without any agglomeration. These results prove that the layered silicates are uniformly distributed in the P(VAc-co-MMA) matrix which might provide a reason for the formation of stable P(VAc-co-MMA)/C30B nanocomposite. In the polymer/clay nanocomposites, dispersion of the nanoparticle is critical because it is the large interface of the individual silicate sheets which allow some of the nanocomposite properties, such as increased T_g, decreased permeability and improved strength and toughness.

Figure 7a, b show the AFM images of the synthesized P(VAc-co-MMA) and P(VAc-co-MMA)/C30B, respectively. The homogeneity of the dispersion of C30B

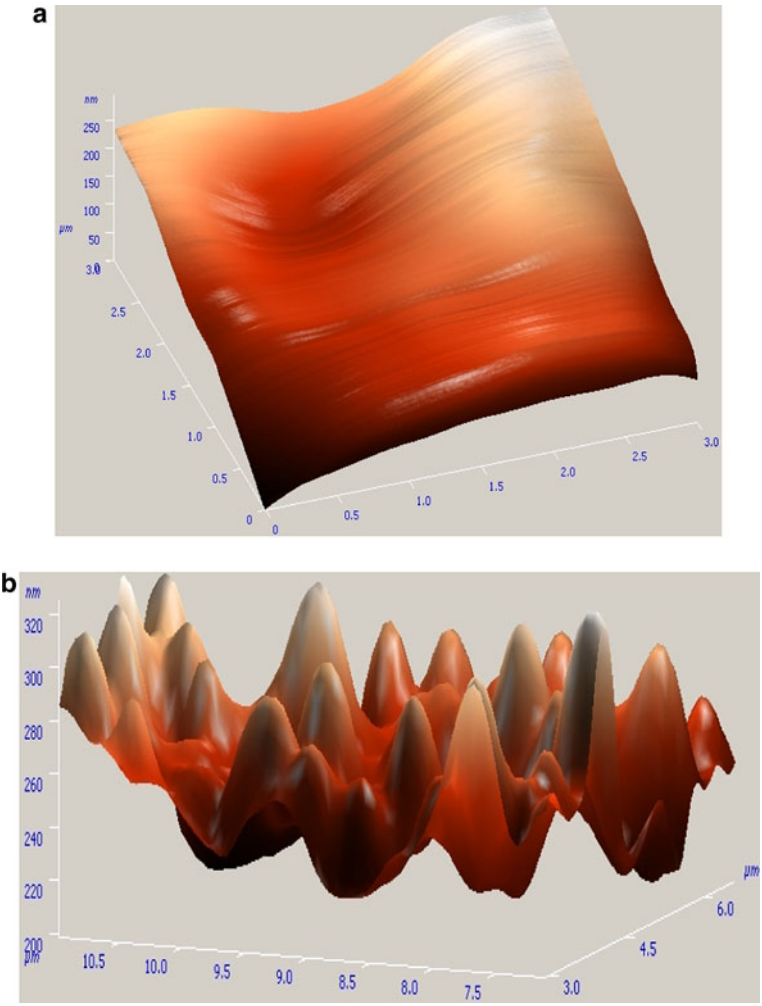

Fig. 7 AFM topographic images, **a** P(VAc-co-MMA), 3 μm × 3 μm × (0–250) nm, **b** P(VAc-co-MMA)/C30B nanocomposite with a C30B concentration of 3%, 3 μm × 4 μm × (0–320) nm

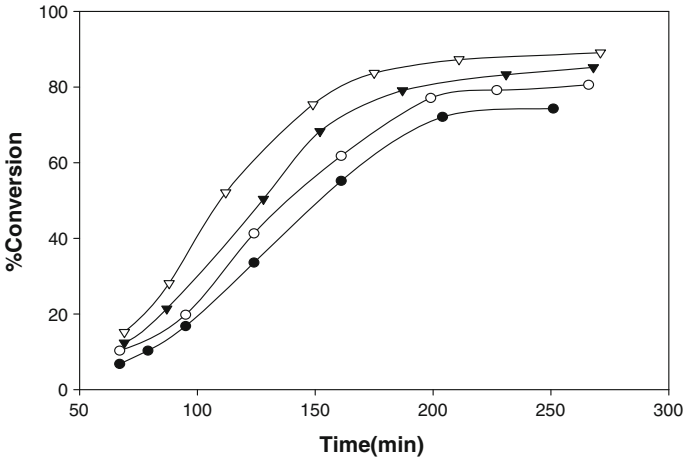

Fig. 8 Effect of clay concentration on the conversion of P(VAc-co-MMA)/C30B with 0% C30B (*filled circle*), 1% C30B (*open circle*), 3% C30B (*filled inverted triangle*), 5% C30B (*open inverted triangle*)

in the nanocomposite was determined by AFM measurements of spin-coated thin films. These figures indicate the effect of C30B presence on the morphology of P(VAc-co-MMA) in the synthesized P(VAc-co-MMA)/C30B nanocomposite. Figure 7b shows homogeneously disperse regions of larger height on top of a smooth P(VAc-co-MMA) copolymer film. These regions have different phase contrast than the P(VAc-co-MMA) matrix indicating the presence of C30B in them.

Figure 8 presents conversion–time plots for copolymerization experiments. It is clear from this figure that at the same condition, polymerization rate (the slope of the curve on the conversion–time plot) can be affected by the presence of C30B. In the case of C30B content of 5%, the rate of polymerization increased significantly. The increase in the polymerization rate is due to the existence of non-agglomerated C30B nanoparticles in the situ emulsion polymerization process which increases the concentration of the active growing chain and the chain propagation rate. Thus, the polymerization rate of nanocomposites is highly increased by increasing the concentration of C30B in the nanocomposite structure.

The conversion–time plot of the synthesized P(VAc-co-MMA)/C30B nanocomposite containing 1% C30B is compared with that for the P(VAc)/C30B nanocomposite [1] in Fig. 9. According to this figure, the polymerization rate and the conversion of the P(VAc-co-MMA)/C30B nanocomposite is much more than those for the P(VAc)/C30B nanocomposite especially after 120 min.

Based on DMTA analysis of the P(VAc-co-MMA)/C30B nanocomposite, the storage modulus for the synthesized copolymer and nanocomposites as a function of temperature is given in Fig. 10. According to this figure, the storage modulus curve for P(VAc-co-MMA) shows a significant drop in modulus but for the P(VAc-co-MMA)/C30B films the drop is more gradual and it occurs at higher temperatures. The tanδ peaks recorded for P(VAc-co-MMA)/C30B nanocomposites have been shifted to higher temperatures compared to the tanδ peak for pure P(VAc-co-MMA),

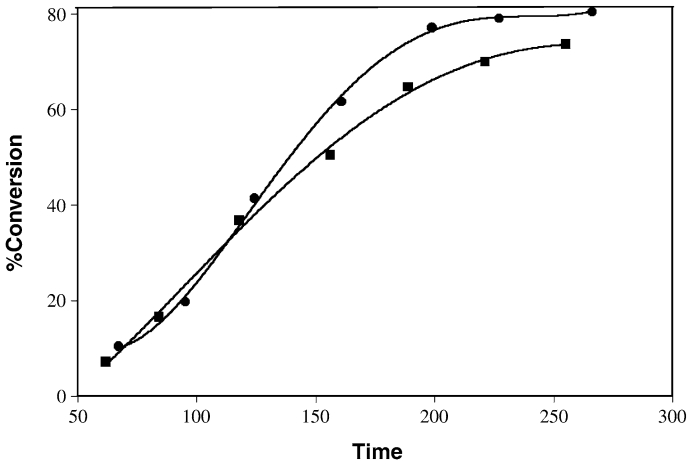

Fig. 9 The conversion–time plot of the synthesized P(VAc-co-MMA)/C30B (*filled circle*) and P(VAc)/C30B (*filled square*) nanocomposites containing 1% C30B

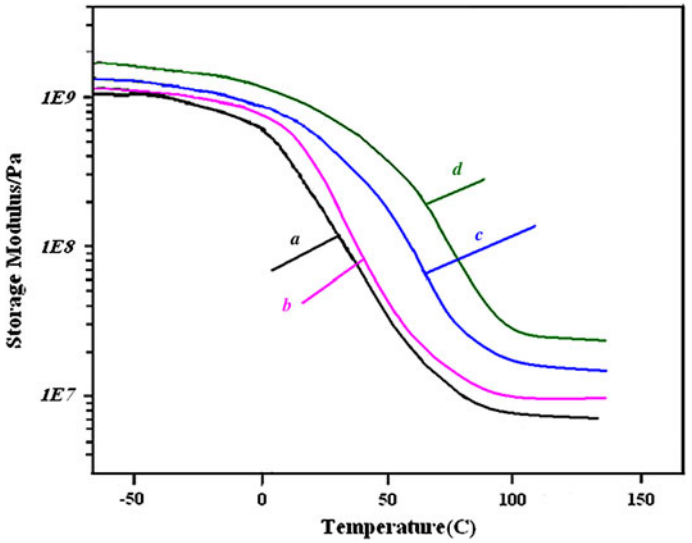

Fig. 10 Storage modulus versus temperature plots for copolymer and its nanocomposites, pure copolymer (*a*); 1% C30B (*b*); 3% C30B (*c*); 5% C30B (*d*)

see Fig. 11. The data are summarized in Table 1. The observed increase in storage modulus as well as a shift in the tanδ peaks to higher temperatures for the P(VAc-co-MMA)/C30B indicates an altered chain mobility of the P(VAc-co-MMA) matrix. As a result, the P(VAc-co-MMA)/C30B nanocomposites have received an increased temperature of use compared to pure P(VAc-co-MMA).

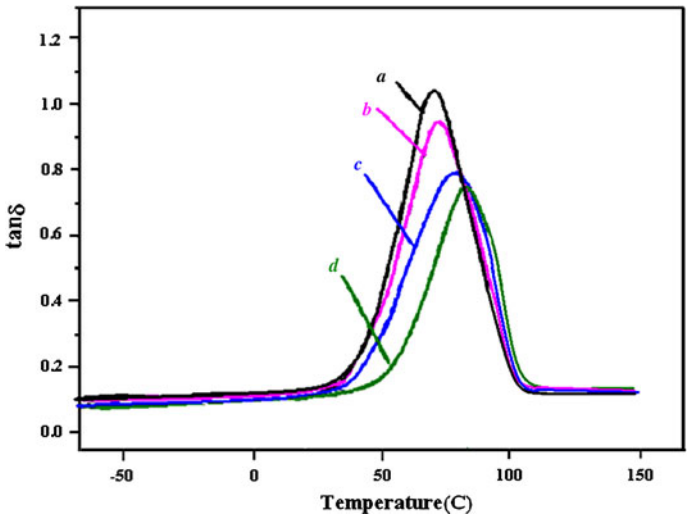

Fig. 11 Tan δ versus temperature for P(VAc-co-MMA) and its P(VAc-co-MMA)/C30B, pure P(VAc-co-MMA) (*a*); 1% C30B (*b*); 3% C30B (*c*); 5% C30B (*d*)

Table 1 Dynamic mechanical thermal properties of copolymer and its nanocomposites

Sample	Storage modulus (GPa)	T_g (°C)
Pure copolymer	1.02	70.38
1% Clay	1.08	71.53
3% Clay	1.27	79.6
5% Clay	1.59	82.8

Conclusions

In summary, the P(VAc-co-MMA)/C30B nanocomposites with various contents of C30B were successfully fabricated via emulsion polymerization. The morphology of P(VAc-co-MMA)/C30B nanocomposites was observed with SEM, TEM, and AFM. The FT-IR and XRD analysis showed that P(VAc-co-MMA) chains have exfoliated into the interlayer of C30B. According to the XRD patterns, copolymer chains have exfoliated into the interlayer of C30B. Due to the intercalation of P(VAc-co-MMA) into galleries of C30B, the *d*-spacing between C30B layers has been increased. The results of SEM analysis of the synthesized P(VAc-co-MMA) nanocomposite with content 3% C30B indicated that the diameter of spherical particles of the copolymer matrix was around 200 nm. To examine the dispersion of the C30B layers in the exfoliated composites, TEM studies were carried out. According to the TEM micrograph of the nanocomposite having 3.0% of C30B, the C30B layers have been exfoliated in the P(VAc-co-MMA) matrix. Based on the obtained results from the conversion–time plots, the polymerization rate and monomer conversion increased with an increase in C30B concentration. The results

from the DMTA showed an improvement in storage modulus over the entire temperature range for P(VAc-co-MMA)/C30B nanocomposites, It was apparent from the DMTA results that all the storage module of the P(VAc-co-MMA)/C30B nanocomposite has the higher storage module than neat P(VAc-co-MMA) below the glass transition temperature (T_g). It was known that the relative values of storage module of the P(VAc-co-MMA)/C30B nanocomposite were influenced by the effective interfacial interaction between the C30B and P(VAc-co-MMA) chains. The tanδ peaks of materials shifted to higher temperatures compared to pure P(VAc-co-MMA). It can therefore be concluded that the nanocomposites were able to increase the temperature of use of copolymer.

References

1. Mohsen-Nia M, Mohammad douladi F (2011) Synthesis and characterization of poly vinyl acetate/montmorillonite nanocomposite by in situ emulsion polymerization technique. Polym Bull 66:1255–1265
2. Iji M, Morishita N, Kai H (2010) Self-assembling siloxane nanoparticles with three phases that increase tenacity of poly L-lactic acid. Polym J 43:101–107
3. Alvi F, Ram M, Gomez H, Joshi R, Kumar A (2010) Evaluating the chemio-physio properties of novel zinc oxide–polyaniline nanocomposite polymer films. Polym J 42:935–940
4. Mohsen-Nia M, Mohammad Doulabi F. PVAc microspheres via semicontinuous emulsion polymerization: synthesis, characterization, kinetic and surface morphology studies. J Adhesion (in press)
5. Araújo PH, Giudici R, Sayer C (2004) Butyl acrylate and vinyl acetate semicontinuous emulsion copolymerization: study of stabilization performance. Macromol Symp 206:179–190
6. Lazaridis N, Alexopoulos AH, Kiparissides C (2001) Semi-batch emulsion copolymerization of vinyl acetate and butyl acrylate using oligomeric nonionic surfactants. Macromol Chem Phys 202: 2614–2619
7. Lee J, Hong C, Choe S, Shim S (2007) Synthesis of polystyrene/silica composite particles by soap-free emulsion polymerization using positively charged colloidal silica. J Colloid Interface Sci 310:112–120
8. Wang Y, Herron N (1992) Photoconductivity of CdS nanocluster-doped polymers. Chem Phys Lett 200:71–75
9. Sahoo PK, Samal R, Swain SK, Rana PK (2008) Synthesis of poly(butyl acrylate) sodium silicate nanocomposite filer retardant. Eur Polym J 44:3522–3528
10. Li Y, Liu L, Zhang W, Fang Y (2004) A new hybrid nanocomposite prepared by graft copolymerization of butyl acrylate onto chitosan in the presence of organophilic montmorillonite. Radiat Phys chem 69:467–472
11. Yildirim EH (2002) Vinyl acetate emulsion polymerization and copolymerization with acrylic monomers. CRC Press, Boca Raton
12. Hao L, Yunzhao Y, Yukun Y (2005) Synthesis of exfoliated polystyrene/montmorillonite nanocomposite by emulsion polymerization using zwitterions as the clay modifier. Eur Polym J 41: 2016–2022
13. Shi Y, Peterson S, Sogah DY (2007) Surfactant-free method for the synthesis of poly(vinyl acetate) masterbatch nanocomposites as a route to ethylene vinyl acetate/silicate nanocomposites. Chem Mater 19:1552–1564